Published in final edited form as:
*Biochemistry*. 2005 August 16; 44(32): 10926–10934. doi:10.1021/bi050645h.

# 2D-measurement of proton $T_{1\rho}$ relaxation in unlabeled proteins: Mobility changes in α-bungarotoxin upon binding of an acetylcholine receptor peptide.†

**Abraham O. Samson**, **Jordan H. Chill**‡, and **Jacob Anglister***
*Department of Structural Biology, Weizmann Institute of Science, Rehovot 76100, Israel.*

## Abstract

A method for the measurement of proton $T_{1\rho}$ relaxation times in unlabeled proteins is described using a variable spin-lock pulse after the initial non-selective 90° excitation in a HOHAHA pulse-sequence. The experiment is applied to α-bungarotoxin (α-BTX) and its complex with a 25-residue peptide derived from the acetylcholine receptor (AChR) α-subunit. A good correlation between high $T_{1\rho}$ values and increased local motion is revealed. In the free form, toxin residues associated with receptor binding according to the NMR structure of α-BTX complex with an AChR peptide and the model for the α-BTX with the AChR display high mobility. Upon binding the AChR peptide a decrease in the relaxation times and motion of residues involved in binding of the receptor α-subunit is exhibited, while residues implicated in binding γ and δ subunits retain their mobility. In addition, the quantitative $T_{1\rho}$ measurements enables us to corroborate the mapping of boundaries of the AChR determinant strongly interacting with the toxin and can similarly be applied to other protein complexes in which peptides represent one of the two interacting proteins. The presented method is advantageous due to its simplicity, generality and time efficiency and paves the way for future investigation of proton relaxation rates in small unlabeled proteins.

### Keywords

epitope mapping; $T_{1\rho}$ relaxation; proton relaxation; dynamics; α-bungarotoxin; acetylcholine receptor

---

NMR relaxation times are influenced by the global tumbling of the molecules as well as by local motions. Such relaxation times include the longitudinal relaxation time ($T_1$), commonly referred to as the laboratory frame spin-lattice relaxation time, the transverse relaxation time ($T_2$), also known as spin-spin relaxation, and the spin-lattice relaxation time in the rotating frame ($T_{1\rho}$) characterized by the decay of magnetization spin-locked by a radio frequency field, $\omega_1=\gamma B_1$, applied perpendicularly to $B_0$. Relaxation of the transverse magnetization in the laboratory frame ($T_2$) and the longitudinal magnetization in the rotating frame ($T_{1\rho}$) also depend on conformational and chemical exchanges.

The efficiency of the relaxation by dipole-dipole interactions, chemical shift anisotropy and scalar interactions, all of which are major contributors to relaxation, depends on the correlation times of the involved nuclei. Protein residues involved in secondary structure usually exhibit

---

†This study was supported by NIH grant NS38301.

*To whom correspondence should be addressed. J.A. is the Dr. Joseph and Ruth Owades Professor of Chemistry. Tel: +972−8−9343394, Fax: +972−8−9344136, E-mail: jacob.anglister@weizmann.ac.il..
‡Present address: Laboratory of Chemical Physics, NIDDK, National Institutes of Health, Bethesda, Maryland 20892 , USA

$T_2$ and $T_{1\rho}$ values that are determined mostly by the overall tumbling rate of the molecule. Flexible regions and unstructured segment of the protein exhibit $T_2$ and $T_{1\rho}$ values that are typically higher than those exhibited by rigid segments (1-3). Ligand binding is often accompanied by altered flexibility of the domains involved in binding, changes that effect local flexibility and therefore can be probed by $T_2$ or $T_{1\rho}$ measurements. Thus measurements of $T_1$, $T_2$, $T_{1\rho}$ and NOE can provide insight into the dynamics of proteins in solution and changes occurring upon ligand binding.

Studies of dynamic processes by NMR have traditionally focused on measurements of the relaxation parameters of $^{15}N$ and $^{13}C$ nuclei bonded to $^{1}H$ using isotope labeled proteins. Proton relaxation times in unlabeled proteins have not been investigated as thoroughly. This can be attributed to several factors, including the difficulty in measurements and data analysis due to spectral overlap. It is also difficult to interpret the $T_2$ and $T_{1\rho}$ data and analyze the type and time scale of motions contributing to relaxation because each proton may relax through several different pathways such as scalar couplings and dipole-dipole interactions with multiple near by protons (4). Nevertheless, several laboratories measured proton relaxation in proteins. Bodenhausen and coworkers (5-7) described several different experiments for measurements of longitudinal and transverse relaxation times of selected protons. These experiments enabled accurate determination of relaxation times of specific protons. However, it was impractical to apply these 1D experiments for measurements of a large number of protons. Arseniev and coworkers successfully measured $T_1$ relaxation times for most of the protons of a small 15-residue peptide gramicidin using a series of inverse-recovery (IR) 2D-COSY experiments (8). In this method, $H^N$, $H^\alpha$, $H^\beta$, and methyl protons were classified into groups with distinctive longitudinal relaxation times. Instead of using a series of 2D measurements with variable intervals during which the magnetization recovers to thermal equilibrium due to longitudinal relaxation, Kay and Prestegard suggested the use of a single 2D “accordion” experiment (9). In this experiment, $T_1$ values were extracted from the line shapes of cross-peaks as described in detail by Bodenhausen and Ernst (10,11). Using such a $T_1$-accordion COSY experiment, the location of divalent ion binding sites in acyl-carrier protein was determined based on relaxation time enhancements following paramagnetic ion replacement (12). In this method, however, not all proton relaxation times were assigned quantitatively. Employing 1D-inverse-recovery experiments, longitudinal relaxation times of amide protons were also measured in a protein that was highly deuterated to avoid relaxation through spin-diffusion (13). A method to monitor DNA rigidity by determining the $T_{1\rho}$ relaxation times of nucleotide protons was described by Wang et al. (14). Several 1D experiments consisting of a 90° pulse followed by a variable-length SL were acquired in order to determine the relaxation values. Schmitz et al. (15) and Kennedy et al. (16) also utilized the rotating frame spin-lattice relaxation to address DNA mobility. $T_1$ and $T_2$ relaxation rates were measured using conventinoal 1D 1R techniques and CPMG experiments. Proton $T_{1\rho}$ relaxation has been utilized to determine internal mobility in glycylglycine (17) and enkephalin (18) and cyclic peptides (19,20). Recently, Schleucher and Wijmenga suggested the use of off-resonance ROESY experiments to detect internal motion in unlabeled proteins in the 100 ps time-scale (21. A series of off-resonance ROESY experiments were applied on BPTI and revealed internal motions of 75 individual long and short range H, H vectors. Torchia and co-workers used amide proton $T_{1\rho}$ measurements in uniformly $^{15}N$-labeled HIV-1 protease to study millisecond time-scale motions (4). To reduce cross-relaxation and obtain relatively larger contribution to relaxation from exchange the protease was uniformly deuterated, thus suppressing most of the cross-relaxation pathways (4). While the multitude of methodologies presented in the aforementioned studies underlines the importance of proton $T_{1\rho}$ measurement, the 1D methods that were used for unlabeled proteins are hopelessly incapable of addressing larger proteins. These studies therefore advocate the need for a simple and general 2D technique by which the $T_{1\rho}$ of all residues in relatively large macromolecule (<12 KDa) could be determined without requiring isotope-labeling.

The nicotinic acetylcholine receptor (AChR) is a ligand-gated cation channel that is activated upon binding of the neurotransmitter acetylcholine (ACh). It is a 290 kDa membrane glycoprotein consisting of five homologous subunits, αδβαγ (22,23), with two ACh binding sites formed at the interface of αδ and αγ subunits (24). The α-subunit of the muscle AChR (α1) also contains a high-affinity binding site for antagonists such as α-bungarotoxin (α-BTX) (25). α-BTX is a 74 amino-acid, 8 kDa α-neurotoxin derived from the snake venom of *Bungarus multicinctus*. It binds strongly to the postsynaptic muscle-AChR with an $IC_{50}$ value of $3.5\times10^{-10}$ M (26), competitively inhibiting ACh binding and thereby blocking neuromuscular transmission. Synthetic peptides analogues corresponding to linear segment of the α-subunit form tight complexes with α-BTX (26-32). The structure of an AChR peptide in complex with α-BTX, a complex containing a total of 99 amino-acid residues, was solved using homonuclear 2D-NMR (33). The overall structure of the toxin consists of a three finger motif with a C-terminal tail. The AChR-peptide folds into a β-hairpin which associates with the triple stranded antiparallel β-sheet core of the toxin to form a five stranded inter-molecular β-sheet. The formation of intermolecular hydrogen bonds together with multiple hydrophobic interactions and cation-π interactions account for the high affinity between the toxin and the AChR peptides. The off-rate of a peptide comprising residues $^{\alpha}$W184-$^{\alpha}$D200 of AChR was found to be $1.1 \times 10^{-4}$ $s^{-1}$ (34).

In the past we have employed differences in $T_{1\rho}$ relaxation times to study protein complexes with peptides. A $T_{1\rho}$-filtered NOESY experiment was used to obtain a transferred-NOE spectrum of a peptide bound to an antibody (35). A 30 ms SL pulse applied after the first 90° pulse eliminated all the cross peaks due to intra-molecular interactions within the 50 kDa antibody Fab fragment and only transferred NOE cross peaks due to antibody-peptide interactions and interactions within the bound peptide were observed (35). In another type of experiment a combination of HOHAHA and ROESY spectra with long mixing period were used to map the epitope of a gp120 V3-loop peptide interacting with an HIV-1 neutralizing antibody (36). Similarly, we mapped the exact segment of an AChR peptide interacting with α-BTX to the segment $^{\alpha}$W184-$^{\alpha}$D200 using NMR dynamic filtering techniques (32) [α-BTX and AChR residues are designated by superscript B or α (i.e $^{B}$X or $^{\alpha}$X) respectively, before the amino-acid type and position in sequence]. HOHAHA and ROESY spectra of the α-BTX/AChR-peptide complex acquired with long mixing times highlighted the peptide residues that did not interact with the toxin and retained considerable mobility upon binding to α-BTX. In these two approaches the duration of the spin lock pulses and the mixing period in the HOHAHA and ROESY experiments were adjusted to obtain optimal discrimination between the protein and the peptide cross peaks. However, there was no attempt to quantitatively characterize the $T_{1\rho}$ relaxation times of the interacting molecules.

Here we present a simple homonuclear 2D method to measure proton $T_{1\rho}$ relaxation times based on the HOHAHA experiment (37). Using this method, we characterized for the first time changes in relaxation times of a snake neurotoxin upon binding an AChR-peptide. A decrease in the relaxation times and the mobility of residues involved in binding of the receptor α-subunit is exhibited, while residues implicated in binding the γ and δ subunits retain their mobility (33. In addition, the quantitative $T_{1\rho}$ measurements enable us to corroborate the mapping of boundaries of the AChR determinant strongly interacting with the toxin.

## EXPERIMENTAL PROCEDURES

### NMR sample preparation

α-BTX was purchased from Sigma and did not require further purification. The toxin was dissolved in 90% $H_2O$/10% $D_2O$ and 0.05% $NaN_3$ and acidified with HCl to pH 4. Final concentration of the α-BTX in the NMR sample was 0.5 mM. The AChR-peptide, EERGWKHWVYYTCCPDTPYLDITEE, corresponding to residues 182−202 of the α1-

subunit of *Torpedo Californica* AChR and elongated with two glutamic acid residues at each terminus to increase solubility, was synthesized and purified as previously described (32). The toxin-peptide complex was prepared and purified as described earlier (32). The purified and lyophilized complex was dissolved in 90% $H_2O$/10% $D_2O$ and 0.05% $NaN_3$ and acidified with HCl to pH 4. Final concentration of the complex in the NMR sample was 2 mM.

### NMR spectroscopy

All NMR spectra were acquired on a Bruker DMX-500 MHz and DRX-800 MHz spectrometer at 30 °C. The experiment used for the 2D $T_{1\rho}$ measurements was based on the HOHAHA pulse sequence (37,38) and incorporated a SL pulse after the initial 90° pulse. The $T_{1\rho}$-filtered HOHAHA spectra were measured utilizing the following pulse sequence:

$$90_x^{o} - SL_y - \text{Evolution} \quad (t_1) - (\text{WALTZ}) - \text{Acquisition} \quad (t_2)$$

Measurements of free α-BTX and its complex with the AChR peptide were performed on an 800 MHz spectrometer. Isotropic mixing was realized using a WALTZ (39) pulse sequence with a short duration of 30 msec. The spectra were acquired using sensitivity enhancement and TPPI, and the water signal was suppressed by the WATERGATE pulse sequence (water suppression by gradient-tailored excitation)(40). Measurements of the AChR-peptide were carried out on a 500 MHz spectrometer.

A series of six experiments was measured with SL durations varying from 0 to 25 msec by 5 msec increments. Complex points acquired on the 500 MHz were 2048 and 256 in the F2 and F1 dimensions, respectively, with spectral widths of 6000 Hz. Complex points acquired on the 800 MHz were 8192 and 800 in the F2 and F1 dimensions respectively with spectral widths of 11160 Hz. All spectra were processed and analyzed using the NMRDraw and NMRPipe programs (41). Unresolved peaks at frequencies close to that of the water required additional baseline correction using polynomial water subtraction in all experiments. Linear prediction in the F1 dimension was also performed to increase resolution and improve the automated peak-picking. Automated peak picking in these spectra was achieved using NMRPipe and in-house Perl scripts. Sequential assignment of the toxin and its peptide complex was performed according to common procedures (42) at 30 °C.

### Data analysis

Proton $T_{1\rho}$ values were determined by fitting the relaxation data to a single exponential decay: $I(t) = I_0 \exp(-t/T_{1\rho})$ using the modelXY package (41). Error values to be included in the calculation were obtained from S/N ratios. Per residue change in accessible surface of the peptide in the α-BTX/AChR-peptide complex (PDB code: 1L4W) was calculated using the homology module of Insight II (Accelrys). Display of the α-BTX/AChR-peptide structure with a radius proportional to the $T_{1\rho}$ value was created using the Molmol program (43).

## RESULTS

### Pulse sequence

The proposed pulse sequence that measures $T_{1\rho}$ values contains a SL pulse after the initial 90° pulse. During this SL pulse, the initial magnetization ($M_0$) is characterized by an exponential decay:

$$M(t_{SL}) = M_0 \quad \exp \quad \left(-t_{SL}/T_{1\rho}\right)$$

During the mixing period further relaxation occurs and the final relaxation is roughly proportional to:

$$M(t_{SL}, \tau_m) = M_0 \quad \exp\left(-t_{SL}/T_{1\rho}\right) \quad \exp\left(-\tau_m/T_{1\rho}\right)$$

The mixing time ($\tau_m$) in the set of experiments is constant and as a result the cross peak intensity decays exponentially according to $T_{1\rho}$ with increasing $t_{SL}$.

The proposed experiment, in which the spin lock pulse is applied before the evolution period, is an extension to two dimensions of the conventional 1D experiment used to measure non-selective $T_{1\rho}$. The 2D experiment has the advantage that it spreads the spectrum of the protein into two dimensions and allows measurements of $T_{1\rho}$ of individual protons in small unlabeled proteins. Other than the increased resolution, the proposed 2D method has the same advantages and drawbacks as the 1D experiment commonly used for non-selective $T_{1\rho}$ measurements.

For long SL pulses proton magnetization may not be characterized by a single exponential decay due to scalar interactions and spin diffusion. Indeed, deviations from single exponential decay were observed utilizing SL pulses of 100 ms and 200 ms. However, the initial relaxation rates measured using short SL pulses are good approximations of the true self-relaxation rates (44,45) and are better characterized by a single exponential decay (44,45). Therefore, short spin lock pulses of up to 25 ms were used herein to obtain $T_{1\rho}$ relaxation times. In addition, a short isotropic mixing time of 25 msec was utilized to minimize signal decay due to magnetization transfer to protons more than three bonds apart. As a result, the $T_{1\rho}$-filtered HOHAHA spectrum displayed strong $H^N/H^\alpha$ cross-peaks and few long range correlations. A section of the HOHAHA spectrum of free α-BTX used for the $T_{1\rho}$ determination is displayed in Figure 1.

The decay of the $H^\alpha(F1)/H^N(F2)$ cross peaks intensity which are above the diagonal is governed by the relaxation rate of $H^\alpha$ protons and the intensity of the cross peaks $H^N(F1)/H^\alpha(F2)$ which are below the diagonal is governed by the relaxation rate of $H^N$ protons. (F2 represents the acquisition dimension.) Since most $H^N(F1)/H^\alpha(F2)$ cross peaks are weakened by the water suppression scheme that dephases water magnetization prior to acquisition, thereby reducing the intensity of all resonances up to 1 ppm away from the water, we concentrated on measuring the decay of the symmetrical cross peaks at frequency $H^\alpha(F1)/H^N(F2)$ governed by the $T_{1\rho}$ relaxation rates of the $H^\alpha$ protons.

## Spectral processing

Well resolved spectra are a prerequisite for the automated peak picking process. As a measure of precaution, the spectral resolution was further increased through processing using squared sine-bell window functions, zero filling, and linear prediction. Without these measures, automated peak picking is less accurate, leading in several cases to poor fits to exponential decay. Signal apodization using a squared cosine-bell window function or a squared-cosine shifted by 45° did not result in any significant changes in the determined $T_{1\rho}$ values

## $T_{1\rho}$ measurements

To calculate the $T_{1\rho}$ values, the decay in cross-peak intensity as a function of the SL pulse was fitted to a mono-exponential curve with minor deviations (Figure 2). The error in peak intensity was estimated at approximately 4% based upon the noise in empty areas of the spectra. Most cross-peaks displayed very good fits to the exponential curve and the estimated error in $T_{1\rho}$ determination was 11% on average. Cross peaks of the geminal protons of glycine residues typically gave rise to two similar $T_{1\rho}$ values. The $T_{1\rho}$ values of few residues that did not give rise to cross-peaks in the spectra (i. e. proline residues and $^B$I1, $^\alpha$E180, the N-terminal residues of the toxin and peptide, respectively) or that were poorly resolved could not be determined. Poorly resolved residues include $^B$T8, $^B$T62 and $^B$D63 in the complex, as well as $^B$S9, $^B$D30, and $^B$A31 in the unbound state.

For the vast majority of the protons a single exponential decay could be easily fitted to the relaxation curve. Deviation from single exponential decay could occur in principle despite the short spin lock pulse if spin diffusion occurs. We assessed the contribution of this possible effect to $T_{1\rho}$ relaxation by repeating our experiment with the spin-lock and evolution blocks reversed (4) as following:

$$90_x^{o} - \text{Evolution } (t_1) - SL_y - \text{(WALTZ)} - \text{Acquisition } (t_2)$$

Since off-diagonal ROESY peaks appeared in this experiment solely for the nearest protons when applying a 25 ms spin lock pulse, we conclude that multi-spin effects are suppressed in our $T_{1\rho}$ measurements, justifying our assumption of monoexponential behavior for the initial relaxation rates.

### $T_{1\rho}$ determination of $H^{\alpha}$ protons of free α-BTX

The $T_{1\rho}$ values of the $H^{\alpha}$ protons of free α-BTX obtained on the 800 MHz are summarized in Figure 3A. The average $T_{1\rho}$ of $H^{\alpha}$ protons in free α-BTX is 50 and 37 msec for all residues and for β-strands' residues respectively. Two segments of the toxin exhibit unusually long $H^{\alpha}T_{1\rho}$ relaxation times (≥100 ms), namely $^{B}$S35 and $^{B}$R36 located at the tip of the second finger, and $^{B}$Q71-$^{B}$G74 at the C-terminus. Moderately long $T_{1\rho}$ relaxation times (≥60 ms) are exhibited by residues at the tip of the first finger, at the tip of the second finger and at the N-terminal strand of the third finger. These results are in agreement with previous model-free based dynamics studies of a three finger toxin that found that the tips of the three fingers as well as the N-terminal segment of the third finger exhibited low order parameters (46, 47).

### $T_{1\rho}$ determination of $H^{\alpha}$ protons of α-BTX in complex with the AChR peptide

The $T_{1\rho}$ values of the $H^{\alpha}$ protons of α-BTX in complex with the AChR peptide are summarized in Figure 3B. The average $T_{1\rho}$ values for all residues and β-strand residues are 35 and 28 msec respectively. The decrease in average $T_{1\rho}$ values in comparison to those obtained for free α-BTX are consistent with the 35% change in molecular weight occurring upon complex formation. Exceptionally large decreases in $T_{1\rho}$ relaxation times are displayed by C-terminal residues $^{B}$K70 (from 64 to 25 msec), $^{B}$Q71 (from 129 to 54 msec), $^{B}$R72 (from 150 to 51 msec), and $^{B}$G74 (from 148 to 50 msec). The decreased mobility of most of the residues at the C-terminal segment in the α-BTX\AChR-peptide complex (Figure 3C) can be explained by the interactions of $^{B}$H68, $^{B}$P69, $^{B}$K70 and $^{B}$Q71 with the AChR peptide (33). In addition to the C-terminus residues, $^{B}$R36 and $^{B}$K38 of the second finger exhibited a dramatic decrease in their $T_{1\rho}$ relaxation time upon binding to the AChR peptide ($^{B}$R36 from 100 to 31 msec, and $^{B}$K38 from 50 to 18 msec) (Figure 3C). A significant decrease of $T_{1\rho}$ is experienced also by the $H^{\alpha}$ proton of $^{B}$C29 (from 50 to 23 msec) which together with $^{B}$K38 extend the β-hairpin of toxin finger II upon complex formation (48). Significant decrease in $T_{1\rho}$ is observed also for residues of the first toxin finger $^{B}$T6 (from 43 to 26 msec), $^{B}$A7 (from 67 to 37 msec) and $^{B}$I11 (from 31 to 21msec) which were found to interact with the AChR peptide. The change in exposed surface upon complex formation of the toxin presented in Figure 3D is correlated with the change in $T_{1\rho}$ relaxation times (Figure 3C). The 2D $T_{1\rho}$ experiment enabled us to determine the relaxation times of several amide protons using the symmetrical $H^{N}$(F1);$H^{\alpha}$(F2) peaks when those were distant enough from the water resonance to be unaffected by solvent suppression. These $T_{1\rho}$ values were similar to those obtained for the $H^{\alpha}$ protons of the corresponding residues.

### $T_{1\rho}$ determination of $H^{\alpha}$ protons of free and α-BTX-bound AChR-peptide

The $T_{1\rho}$ profile of the AChR-peptide in its free form is presented in Figure 4A. The peptide exhibits relatively long relaxation times with an average $T_{1\rho}$ of 155 msec. Most of the peptide residues, excluding the C-terminal residue, display $T_{1\rho}$ relaxation times of 90 to 160 msec. The

C-terminal segment, $^{\alpha}$D200-$^{\alpha}$E204, exhibits gradually increasing $T_{1\rho}$ values, ranging from 204 msec for $^{\alpha}$D200 to 352 msec for$^{\alpha}$E204. The low relaxation rates and therefore long relaxation times at the termini are typical of a small polymer and peptides with unrestrained termini (49, 50).

The $T_{1\rho}$ measurements of the AChR peptide in complex with α-BTX presented in Figure 4B confirm the previous mapping of the AChR determinant (32). The $T_{1\rho}$ values of the AchR peptide vary from 100 msec for $^{\alpha}$E204 down to 21.9 and 20.3 msec for αL199 and $^{\alpha}$K185 respectively. Residues outside the binding determinant (excluding residue $^{\alpha}$G183 referred to below), namely $^{\alpha}$E181, $^{\alpha}$182, $^{\alpha}$W184, $^{\alpha}$I201, $^{\alpha}$T202, $^{\alpha}$E203 and $^{\alpha}$E204 exhibit $T_{1\rho}$ values above an arbitrary threshold value of 45 msec. Residues within the binding determinant, $^{\alpha}$K185-$^{\alpha}$D200, with the exception of $^{\alpha}$D195, display $T_{1\rho}$ values under 45 msec (Figure 4B), similar to most of the toxin protons. These values quantitatively define the residues constituting the binding determinant of the AChR and account for their absence in the $T_{1\rho}$-attenuated HOHAHA and ROESY experiments. Interestingly, $^{\alpha}$D195 exhibits increased $T_{1\rho}$ of 52 msec that can be correlated with the absence of interactions with the toxin and the inferred flexibility of this residue. $^{\alpha}$D195 and $^{\alpha}$T196 were found to form a β-bulge in complex with the toxin and no interactions between them and the toxin could be detedted, thus explaining the increased $T_{1\rho}$ values observed for these two residues close to the center of the AChR determinant interacting with the toxin (33). In general the change in exposed surface upon binding of the AChR-peptide presented in Figure 4C is correlated with the change in $T_{1\rho}$ times (Figures 4A and 4B).

## $T_{1\rho}$ of glycine residues

Glycine residues exhibit short $T_{1\rho}$ values which differ considerably from those of their adjacent residues due to the strong dipole-dipole interactions between the geminal $H^{\alpha}$ protons. Nevertheless, glycine $T_{1\rho}$ values display the same correlation with the α-BTX structure. Thus glycines $^{B}$G19, $^{B}$G37, and $^{B}$G43, located in the structured regions of the complex, exhibit an average $T_{1\rho}$ of 17 msec in the bound state. In contrast, $T_{1\rho}$ values of toxin residue $^{B}$G74 (50 msec) and peptide residue $^{\alpha}$G183 (34 msec) located at the termini of the toxin and peptide, respectively, have far longer $T_{1\rho}$ values. We therefore conclude that a comparison between glycine residues at the different positions in the complex can be used to qualitatively evaluate the variation in their dynamics.

## A simplified spectrum for $T_{1\rho}$ measurements of mobile residues obtained using a long WALTZ pulse-train

In complexes of large proteins with peptide ligands the overlap with the protein cross peaks would hamper quantitative $T_{1\rho}$ measurements of the flexible segments of the peptide that do not interact with the protein. Elimination of the protein cross peaks as well as cross peaks of the peptide residues strongly interacting with the protein could be achieved by increasing the duration of the WALTZ pulse trains. To demonstrate the feasibility of $T_{1\rho}$ measurements of flexible domains in large protein and their complexes we determined the $T_{1\rho}$ relaxation times when the duration of the WALTZ pulse train is 100 ms and 200 ms and compared the results to those obtained when the duration of the WALTZ is 30 ms. No significant changes in the $T_{1\rho}$ values were observed when different duration of the WALTZ is used. However, a 200 ms WALTZ eliminated most of the background from α-BTX and highlighted the residues of the peptide that do not interact with the toxin and the mobile regions in the toxin itself (Figure 5). Thus, long WALTZ trains can be used to simplify the spectra and enable more accurate epitope mapping and quantitative determination of $T_{1\rho}$ in flexible domains possibly even for large proteins and their complexes.

### Comparison of $T_{1\rho}$ values obtained by 1D

To further validate the proposed method we determined the $T_{1\rho}$ values of five amide protons ($^{B}$K70, $^{B}$K64, $^{B}$K26, $^{B}$C29, $^{\alpha}$V188) as well as three $H^{\alpha}$ protons ($^{B}$M27, $^{B}$Y24, $^{B}$C23) that are well resolved in the 1D spectrum. The conventional 1D pulse sequence ($90°_{x}$-$SL_{y}$−$180°_{x}$) was used for that purpose. These amide and $H^{\alpha}$ $T_{1\rho}$ values were compared to the $T_{1\rho}$ values of the $H^{\alpha}$ protons of the corresponding residues measured by the 2D pulse sequence. The 1D values deviate from their 2D counterparts by an average of ± 8% which is within the experimental error.

### Comparison of $T_{1\rho}$ values obtained by 2D using two different spin lock power

The measured $T_{1\rho}$ values are sensitive to exchange processes, for example equilibrium between two conformations, occurring in millisecond timescale (17,51. To check the reproducibility of the $T_{1\rho}$ measurements and to rule out any significant exchange contribution to the measured relaxation rates we repeated the $T_{1\rho}$ measurements using 5 kHz spin lock power. Most importantly, the overall $T_{1\rho}$ profile is very similar to that measured with a spin lock of 8.3 kHz, suggesting that there is no significant contribution of exchange processes to the relaxation. The systematic increase of 10% in $T_{1\rho}$ values is expected due to the smaller tilt angle of the rotating frame when applying a weaker SL pulse (52)

## Discussion

### Comparison with relaxation studies of other α-neurotoxins

Three finger toxins have been the focus of numerous studies. Interest in this family of toxins has been motivated mainly by their high affinity binding to AChR. The dynamics of few snake three-finger neurotoxins in their free form only were studied by NMR. The dynamics of the three-finger short snake neurotoxin toxin (46) and the long neurotoxin LSIII (53) were studied in detail by NMR using natural abundance $^{13}$C and by molecular dynamics. The dynamics of toxin α was studied also using $^{15}$N labeled protein (54). The largest mobility, as reflected by the NMR order parameters and by molecular dynamics simulations, was found for residues at the tip of the second finger. Using model-free analysis this region was characterized by large amplitude motions in the pico- and nano-second time scale (53). The C-terminal segment was found to be rigid in the short neurotoxin toxin α and highly mobile in the long-neurotoxin LSIII. The other regions that exhibited high flexibility were the tip of loop I and the N-terminal strand of loop III and the tip of this loop. This is in excellent agreement with the unusually long $T_{1\rho}$ relaxation times (≥ 100 ms) observed in this study for $^{B}$S35 and $^{B}$R36 at the tip of the second finger (Figure 6) and for $^{B}$Q71, $^{B}$R72 and $^{B}$G74 at the C-terminus. The higher than average $T_{1\rho}$ relaxation times (≥ 60 msec) observed for residues at the tip of the first finger and at the third finger is also in good agreement with the earlier dynamics studies.

### Changes in toxin mobility upon binding the AChR peptide

In the absence of a three dimensional structure of the complexes of toxin α and LSIII with AChR or AChR peptides, mutational analysis was previously used to locate the segments of these toxins involved in binding. Correlation has been found between the toxins' segments implicated in binding and the flexibility observed by NMR. The NMR structure of α-BTX complex with the AChR peptide, and the derived model for α-BTX complex with the extracellular domain of the receptor, enable for the first time to compare the $T_{1\rho}$ relaxation times of the free toxin to those of the bound toxin and derive correlations between changes in relaxation times and interactions with AChR.

Upon binding the AChR-peptide, the average $T_{1\rho}$ of α-BTX in the β-strands decreases from 37 msec to 28 msec ($T_{1\rho}$ ratio of 1.32) mostly due to the increase of the molecular mass from

~8 kDa to ~11.1 kDa. The $T_{1\rho}$ ratios are comparable to the reciprocal of the molecular weight ratio (1.39). As reflected by the $T_{1\rho}$ values in Figure 3, several larger than average changes in the toxin relaxations times occur upon binding the αAChR-peptide. The major change occurs in residues $^{B}$T6, $^{B}$A7, and $^{B}$I11 of the first finger, in $^{B}$R36 and $^{B}$K38 of second fingertip and in $^{B}$K70-$^{B}$G74 of the C-terminus. All residues exhibiting considerably larger than average decrease in $T_{1\rho}$ coincide with the toxin regions shown to interact with the AChR peptide, namely $^{B}$S5-$^{B}$T12, $^{B}$R36-$^{B}$L42, and $^{B}$H68-$^{B}$Q71 (33). The observed changes in $T_{1\rho}$ probably reflect a significant change in mobility due to interactions with the AChR peptide. Residues located at the tip of toxin finger I play an important role in binding the AChR-peptide. Upon binding, the increase in fraction of buried surface of residues $^{B}$T6, $^{B}$A7, and $^{B}$I11 are 23%, 67% and 13% respectively (33). These residues were also shown to form multiple interactions with peptides and mimotopes of the major interacting determinant of the α-subunit of AChR (33,48,55-58). $^{B}$R36 is one of the very few invariant residues in snake α-neurotoxins, and it was previously suggested to mimic acetylcholine in its interactions with AChR (33,59,60). The decrease in the $T_{1\rho}$ relaxation time of $^{B}$R36 can be explained by its extensive interactions with $^{\alpha}$Y190 and $^{\alpha}$Y198 of the AChR peptide (33). $^{B}$K38 was found to interact with $^{\alpha}$Y190 and $^{\alpha}$T191. Moreover, upon the binding of the AChR peptide to α-BTX the C-terminal β-strand of α-BTX second finger is elongated and the segment $^{B}$K38-$^{B}$V40 which is part of the elongated β-strand forms intermolecular β-sheet with the β-hairpin formed by the AChR peptide. The formation of the intermolecular β-sheet should contribute to the dramatic change in the relaxation properties of $^{B}$K38. C-terminal residues $^{B}$H68-$^{B}$Q71 interact strongly with the AChR-peptide. Upon binding, residues $^{B}$H68, $^{B}$K70 and $^{B}$Q71 experience an increase in fraction of buried surface of 12%, 36% and 41% respectively (33) in accord with the decrease of $T_{1\rho}$. The C-terminal segment was also found to form many interactions in structural studies of α-BTX complexes with AChR peptides and mimotopes (33,48,55-58,61) and truncation of C-terminal residues $^{B}$H68-$^{B}$G74 leads to a seven fold decrease in apparent binding affinity to the receptor (60).

## Biological role of toxin fingertip dynamics

The NMR structure of α-BTX with the AChR peptide and the NMR derived model for AChR complex with α-BTX revealed for the first time that the invariant $^{B}$R36 occupies the binding site for acetylcholine (33). This is contraty to suggestions that neurotoxins did not bind to the ACh binding site but rather sterically covered the entrance to the ligand binding pocket (53, 56). The ACh binding sites are located in two deep pockets at the interface of αγ- and αδ-subunits. The flexibility of $^{B}$R36 along with that of the invariant glycine $^{B}$G37 on the second fingertip is probably required for the penetration of the arginine side chain into this deep pocket and for optimal fit. The flexibility of the C-terminal segment which wraps the AChR β-hairpin formed by residues 184−200 may be required for optimal binding. Interestingly, five residues retained considerably long $T_{1\rho}$ relaxation times in the bound toxin, indicative of considerable mobility (Figure 3B & 6). These residues comprise $^{B}$S34 and $^{B}$S35 at the tip of second finger as well as $^{B}$S50, $^{B}$K51 and $^{B}$Y54 at the N-terminal strand of the third finger. These residues were not found to interact with the AChR peptide and do not display exceptional changes in their relaxation times (Figure 3C). However, these five residues were predicted to interact with the γ and δ subunits in the NMR-derived model of the hetero-pentameric AChR complex with α-BTX (33). The flexibility of the residues involved in AChR binding could be important for optimal fit with AChR of different species and for the penetration of the second finger into the cleft between the αγand αδ subunit and the insertion of $^{B}$R36 into the deep and partially concealed pocket that serves for acetylcholine binding.

## Applications

Proton magnetic relaxation measurements do not enjoy widespread popularity, perhaps because current 1D methods suffer from poor resolution and are suitable only for short peptides.

Herein, we presented a simple 2D method to measure $T_{1\rho}$ relaxation of protons in unlabeled proteins. The proposed experiment will facilitate the determination of the proton relaxation rates in unlabeled proteins. Comparison of the results of the $T_{1\rho}$ measurements with model-free analysis and molecular dynamics studies of neurotoxins reveals correlation between proton $T_{1\rho}$ relaxation times that are considerably longer than the average $T_{1\rho}$ of the other protein protons with large amplitude motion in the pico- to nano-second time scale. Thus proton $T_{1\rho}$ measurements can be used to obtain qualitative information about segments of the proteins that are unstructured or have unusual flexibility. As such, $T_{1\rho}$ measurements can be used to define the boundaries of epitopes within longer peptides that interact strongly with antibodies, receptors or other proteins.

## Acknowledgement

We thank Profs. Fred Naider and Eva Meirovitch, for helpful comments and assistance in the preparation of this manuscript. J.A. is the Dr. Joseph and Ruth Owades Professor of Chemistry. This study was supported by NIH grant NS38301.

## Abbreviations

1D, One-dimensional
2D, Two-dimensional
α-BTX, α-bungarotoxin
ACh, Acetylcholine
AChR, Acetylcholine receptor
COSY, Correlation spectroscopy
CPMG, Carr-Purcell-Meiboom-Gill experiment
HOHAHA, Homonuclear Hartman Hahn spectroscopy
IR, Inverse recovery
NMR, Nuclear magnetic resonance
NOESY, Nuclear Overhauser enhancement spectroscopy
ROESY, Rotating frame Overhauser spectroscopy
SL, Spin lock
$T_1$, Spin-lattice, longitudinal relaxation time in the laboratory frame
$T_{1\rho}$, Spin-lattice, longitudinal relaxation time in the rotating frame
$T_2$, Spin-spin, transverse relaxation time
TOCSY, Total correlation spectroscopy

## References

1. Torchia D, Lyerla J, Quattrone AJ. Molecular dynamics and structure of the random coil and helical states of the collagen peptide, α1-CB2, as determined by $^{13}C$ magnetic resonance. Biochemistry 1975;14:887–900. [PubMed: 1125175]
2. Jardetzky, O.; Roberts, GCK. NMR in molecular biology. Academic Press, Inc.; New York: 1981.
3. Weiss MA, Eliason JL, States DJ. Dynamic filtering by two-dimensional $^1H$ NMR with application to phage λ repressor. Proc. Natl. Acad. Sci. U S A 1984;81:6019–23. [PubMed: 6237367]
4. Ishima R, Wingfield PT, Stahl SJ, Kaufman JD, Torchia DA. Using amide $^1H$ and $^{15}N$ transverse relaxation to detect millisecond time-scale motions in perdeuterated proteins: application to HIV-1 protease. J. Am. Chem. Soc 1998;120:10534–42.
5. Boulat B, Bodenhausen G. Measurement of proton relaxation rates in proteins. J. Biomol. NMR 1993;3:335–348.
6. Millet O, Chiarparin E, Pelupessy P, Pons M, Bodenhausen G. Measurement of relaxation rates of $N^H$ and $H^\alpha$ backbone protons in proteins with tailored initial conditions. J. Magn. Reson 1999;139:434–8. [PubMed: 10423382]

7. Boulat B, Konrat R, Burghardt I, Bodenhausen G. Measurement of relaxation rates in crowded NMR spectra by selective coherence transfer. J. Magn. Reson 1992;114:5412–5414.
8. Arseniev AS, Sobol AG, Bystrov VF. $T_1$ relaxation measurement by two-dimensional NMR spectroscopy. J. Mol. Graph 1986;70:427–435.
9. Kay LE, Prestegard JH. Spin-lattice relaxation rates of coupled spins from 2D accordion spectroscopy. J. Magn. Reson 1988;77:599–605.
10. Bodenhausen G, Ernst RR. The accordion experiment, a simple approach to three-dimensional NMR spectroscopy. J. Magn. Reson 1981;45:367.
11. Bodenhausen G, Ernst RR. Direct determination of rate constants of slow dynamic processes by two-dimensional “accordion” spectroscopy in nuclear magnetic resonance. J. Am. Chem. Soc 1982;104:1304.
12. Frederick AF, Kay LE, Prestegard JH. Location of divalent ion sites in acyl carrier protein using relaxation perturbed 2D NMR. FEBS Lett 1988;238:43–8. [PubMed: 3049158]
13. Ulmer TS, Campbell ID, Boyd J. Amide proton relaxation measurements employing a highly deuterated protein. J. Magn. Reson 2004;166:190–201. [PubMed: 14729031]
14. Wang YS, Ikuta S. Proton on-resonance rotating frame spin-lattice relaxation measurements of B and Z double-helical oligodeoxyribonucleotides in solution. J. Am. Chem. Soc 1989;111:1243–8.
15. Schmitz U, Sethson I, Egan WM, James TL. Solution structure of a DNA octamer containing the Pribnow box via restrained molecular dynamics simulation with distance and torsion angle constraints derived from two-dimensional nuclear magnetic resonance spectral fitting. J. Mol. Biol 1992;227:510–31. [PubMed: 1404366]
16. Kennedy MA, Nuutero ST, Davis JT, Drobny GP, Reid BR. Mobility at the TpA cleavage site in the T3A3-containing AhaIII and PmeI restriction sequences. Biochemistry 1993;32:8022–35. [PubMed: 8347604]
17. Bleich HE, Glasel JA. Rotating frame spin-lattice relaxation experiments and the problem of intramolecular motions of peptides in solution. Biopolymers 1978;17:2445–57.
18. Bleich HE, Day AR, Freer RJ, Glasel JA. NMR rotating frame relaxation studies of intramolecular motion in peptides. Tyrosine ring motion in methionine-enkephalin. Biochem. Biophys. Res. Commun 1979;87:1146–53. [PubMed: 465030]
19. Kopple K, Bhandary KK, Kartha G, Wang YS, Parameswaran KN. Conformations of cyclic octapeptides. 3. Cyclo-(D-Ala-Gly-Pro-Phe)$_2$. Conformations in crystals and a $T_{1\rho}$ examination of internal mobility in solution. J. Am. Chem. Soc 1986;108:4637–4642.
20. Kopple K, Wang SY, Cheng AG, Bhandary KK. Conformations of cyclic octapeptides. 5. Crystal structure of cyclo(Cys-Gly-Pro-Phe)$_2$ and rotating frame relaxation ($T_{1\rho}$) NMR studies of internal mobility in cyclic octapeptides. J. Am. Chem. Soc 1988;110:4168–76.
21. Scheucher J, Wijmenga SS. How to detect internal motion by homonuclear NMR. J. Am. Chem. Soc 2002;124:5881–9. [PubMed: 12010063]
22. Karlin A. Structure of nicotinic acetylcholine receptors. Curr Opin Neurobiol 1993;3:299–309. [PubMed: 8369624]
23. Corringer PJ, Le Novere N, Changeux JP. Nicotinic receptors at the amino acid level. Annu. Rev. Pharmacol. Toxicol 2000;40:431–58. [PubMed: 10836143]
24. Blount P, Merlie JP. Molecular basis of the two nonequivalent ligand binding sites of the muscle nicotinic acetylcholine receptor. Neuron 1989;3:349–57. [PubMed: 2642001]
25. Haggerty JG, Froehner SC. Restoration of $^{125}$I-alpha-bungarotoxin binding activity to the alpha subunit of Torpedo acetylcholine receptor isolated by gel electrophoresis in sodium dodecyl sulfate. J. Biol. Chem 1981;256:8294–7. [PubMed: 7263653]
26. Wilson PT, Hawrot E, Lentz TL. Distribution of α-bungarotoxin binding sites over residues 173-204 of the alpha subunit of the acetylcholine receptor. Mol. Pharmacol 1988;34:643–50. [PubMed: 3193956]
27. Wilson PT, Lentz TL, Hawrot E. Determination of the primary amino acid sequence specifying the α-bungarotoxin binding site on the α subunit of the acetylcholine receptor from Torpedo californica. Proc. Natl. Acad. Sci. U S A 1985;82:8790–4. [PubMed: 3866252]

28. Wilson PT, Lentz TL. Binding of α-bungarotoxin to synthetic peptides corresponding to residues 173-204 of the α subunit of Torpedo, calf, and human acetylcholine receptor and restoration of high-affinity binding by sodium dodecyl sulfate. Biochemistry 1988;27:6667–74. [PubMed: 3196679]
29. Ralston S, Sarin V, Thanh HL, Rivier J, Fox JL, Lindstrom J. Synthetic peptides used to locate the α-bungarotoxin binding site and immunogenic regions on α subunits of the nicotinic acetylcholine receptor. Biochemistry 1987;26:3261–6. [PubMed: 2443159]
30. Conti-Tronconi BM, Tang F, Diethelm BM, Spencer SR, Reinhardt-Maelicke S, Maelicke A. Mapping of a cholinergic binding site by means of synthetic peptides, monoclonal antibodies, and α-bungarotoxin. Biochemistry 1990;29:6221–30. [PubMed: 2207067]
31. Neumann D, Barchan D, Safran A, Gershoni JM, Fuchs S. Mapping of the α-bungarotoxin binding site within the α subunit of the acetylcholine receptor. Proc. Natl. Acad. Sci. U S A 1986;83:3008–11. [PubMed: 3458258]
32. Samson AO, Chill JH, Rodriguez E, Scherf T, Anglister J. NMR mapping and secondary structure determination of the major acetylcholine receptor α-subunit determinant interacting with α-bungarotoxin. Biochemistry 2001;40:5464–73. [PubMed: 11331011]
33. Samson A, Scherf T, Eisenstein M, Chill J, Anglister J. The mechanism for acetylcholine receptor inhibition by α-neurotoxins and species-specific resistance to α-bungarotoxin revealed by NMR. Neuron 2002;35:319–32. [PubMed: 12160749]
34. Aronheim A, Eshel Y, Mosckovitz R, Gershoni JM. Characterization of the binding of α-bungarotoxin to bacterially expressed cholinergic binding sites. J. Biol. Chem 1988;263:9933–7. [PubMed: 3290216]
35. Scherf T, Anglister J. A $T_{1\rho}$-filtered two-dimensional transferred NOE spectrum for studying antibody interactions with peptide antigens. Biophys. J 1993;64:754–61. [PubMed: 8386014]
36. Zvi A, Kustanovich I, Feigelson D, Levy R, Eisenstein M, Matsushita S, Richalet-Secordel P, Regenmortel MH, Anglister J. NMR mapping of the antigenic determinant recognized by an anti-gp120, human immunodeficiency virus neutralizing antibody. Eur. J. Biochem 1995;229:178–87. [PubMed: 7538073]
37. Braunschweiler L, Ernst RR. Coherence transfer by isotropic mixing: application to proton correlation spectroscopy. J. Mag. Res 1983;53:521–8.
38. Bax A, Davis DG. MLEV-17-based two-dimensional homonuclear magnetization transfer spectroscopy. J. Mag. Res 1985;65:335.
39. Shaka AJ, Keeler J, Freeman R. Evaluation of a new broadband decoupling sequence: WALTZ-16. J. Mag. Res 1983;53:313–340.
40. Piotto M, Saudek V, Sklenar V. Gradient-tailored excitation for single-quantum NMR spectroscopy of aqueous solutions. J. Biomol. NMR 1992;2:661–5. [PubMed: 1490109]
41. Delaglio F, Grzesiek S, Vuister GW, Zhu G, Pfeifer J, Bax A. NMRPipe: a multidimensional spectral processing system based on UNIX pipes. J. Biomol. NMR 1995;6:277–93. [PubMed: 8520220]
42. Wüthrich, K. NMR of Proteins and Nucleic Acids. Wiley; New York: 1986.
43. Koradi R, Billeter M, Wuthrich K. MOLMOL: a program for display and analysis of macromolecular structures. J. Mol. Graph 1996;14:51–5. 29–32. [PubMed: 8744573]
44. Werbelow LG, Grant DM. Intramolecular dipolar relaxation in multispin systems. Adv. Magn. Reson 1977;9:189–299.
45. Vold RL, Vold RR. Nuclear magnetic relaxation in coupled spin systems. Progress in NMR Spectroscopy 1978;12:79–113.
46. Guenneugues M, Gilquin B, Wolff N, Menez A, Zinn-Justin S. Internal motion time scales of a small, highly stable and disulfide-rich protein: a $^{15}N$, $^{13}C$ NMR and molecular dynamics study. J. Biomol. NMR 1999;14:47–66. [PubMed: 10382305]
47. Gilquin B, Bourgoin M, Menez R, Le Du MH, Servent D, Zinn-Justin S, Menez A. Motions and structural variability within toxins: implication for their use as scaffolds for protein engineering. Protein Sci 2003;12:266–77. [PubMed: 12538890]
48. Basus VJ, Song G, Hawrot E. NMR solution structure of an α-bungarotoxin/nicotinic receptor peptide complex. Biochemistry 1993;32:12290–8. [PubMed: 8241115]

49. Finerty PJ Jr. Mittermaier AK, Muhandiram R, Kay LE, Forman-Kay JD. NMR dynamics-derived insights into the binding properties of a peptide interacting with an SH2 domain. Biochemistry 2005;44:694–703. [PubMed: 15641795]
50. Valeur B, Jarry J, Geny F, Monnerie L. Dynamics of macromolecular chains. II. Orientation relaxation generated by elementary three-bond motions and notion of an independent kinetic segment. J. Polym. Sci., Part B. Polym. Phys 1975;13:675–82.
51. Deverell C, Morgan RE, Strange JH. Studies of chemical exchange by nuclear magnetic relaxation in the rotating frame. Mol. Phys 1970;18:553–9.
52. Cavanagh, J.; Fairbrother, WJ.; Palmer, AG.; Skelton, NJ. Protein NMR spectroscopy: Principles and practice. Academic press, inc.; San Diego: 1996.
53. Connolly PJ, Stern AS, Turner CJ, Hoch JC. Molecular dynamics of the long neurotoxin LSIII. Biochemistry 2003;42:14443–51. [PubMed: 14661955]
54. Guenneugues M, Drevet P, Pinkasfeld S, Gilquin B, Menez A, Zinn-Justin S. Picosecond to hour time scale dynamics of a ”three finger” toxin: correlation with its toxic and antigenic properties. Biochemistry 1997;36:16097–108. [PubMed: 9405043]
55. Scarselli M, Spiga O, Ciutti A, Bernini A, Bracci L, Lelli B, Lozzi L, Calamandrei D, Di Maro D, Klein S, Niccolai N. NMR structure of α-bungarotoxin free and bound to a mimotope of the nicotinic acetylcholine receptor. Biochemistry 2002;41:1457–63. [PubMed: 11814338]
56. Harel M, Kasher R, Nicolas A, Guss JM, Balass M, Fridkin M, Smit AB, Brejc K, Sixma TK, Katchalski-Katzir E, Sussman JL, Fuchs S. The binding site of acetylcholine receptor as visualized in the x-ray structure of a complex between α-bungarotoxin and a mimotope peptide. Neuron 2001;32:265–75. [PubMed: 11683996]
57. Scherf T, Balass M, Fuchs S, Katchalski-Katzir E, Anglister J. Three-dimensional solution structure of the complex of α-bungarotoxin with a library-derived peptide. Proc. Natl. Acad. Sci. U S A 1997;94:6059–64. [PubMed: 9177168]
58. Scherf T, Kasher R, Balass M, Fridkin M, Fuchs S, Katchalski-Katzir E. A β-hairpin structure in a 13-mer peptide that binds α-bungarotoxin with high affinity and neutralizes its toxicity. Proc. Natl. Acad. Sci. U S A 2001;98:6629–34. [PubMed: 11381118]
59. Karlsson, E. Handbook of experimental pharmacology. Lee, CY., editor. Springer Verlag; Berlin: p. 159-212.
60. Rosenthal JA, Levandoski MM, Chang B, Potts JF, Shi QL, Hawrot E. The functional role of positively charged amino acid side chains in α-bungarotoxin revealed by site-directed mutagenesis of a His-tagged recombinant α-bungarotoxin. Biochemistry 1999;38:7847–55. [PubMed: 10387025]
61. Zeng H, Moise L, Grant MA, Hawrot E. The solution structure of the complex formed between α-bungarotoxin and an 18mer cognate peptide derived from the α1 subunit of the nicotinic acetylcholine receptor from torpedo californica. J. Biol. Chem 2001;18:18.

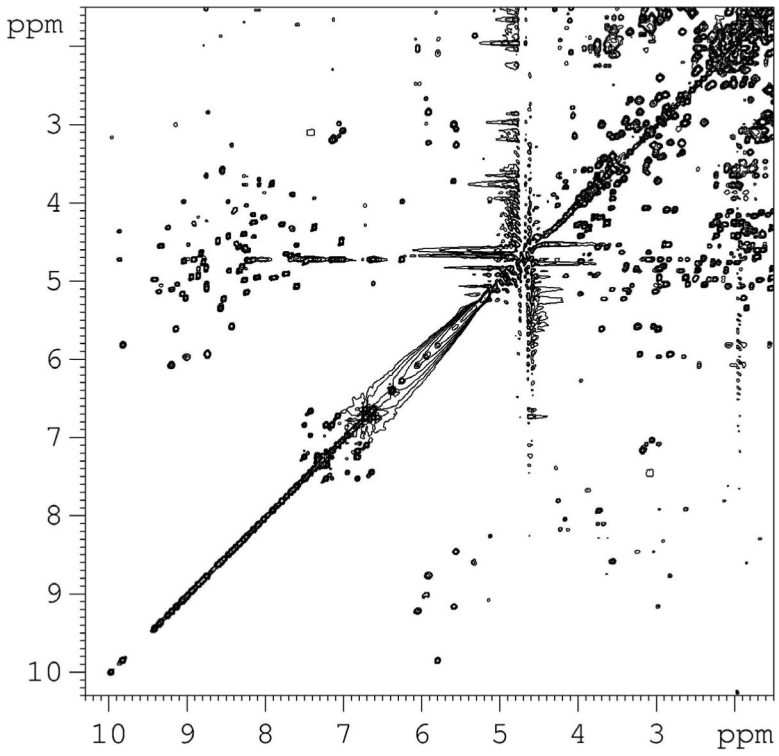


**Figure 1.**

$T_{1\rho}$-filtered HOHAHA spectrum of free α-BTX. The spectrum was measured on an 800 MHz spectrometer at 30°C with a spin-lock pulse applied after the initial 90° pulse. The duration of the spin-lock pulse was 25 msec. Notice the absence of the majority of the $H^N(F2)/H^\alpha(F1)$ cross-peaks due to the water suppression scheme.

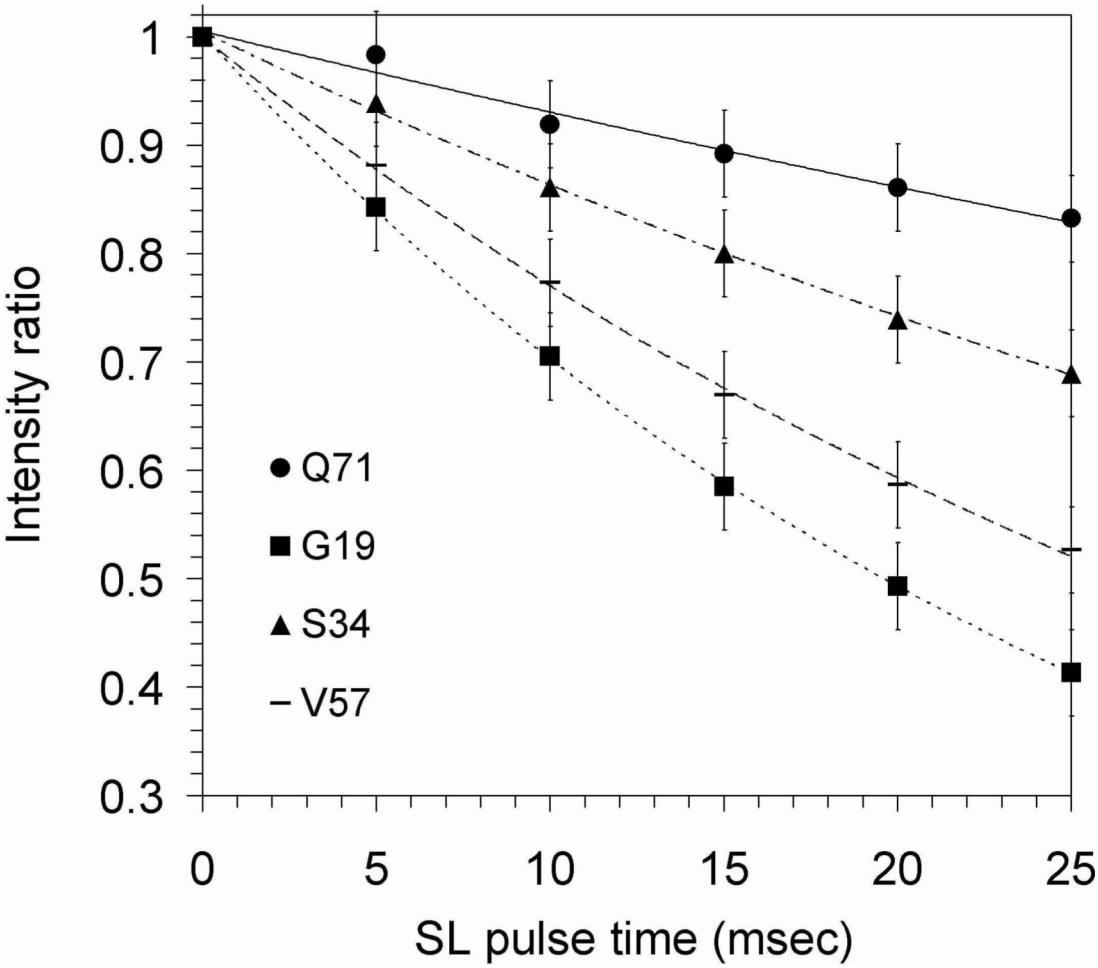


**Figure 2.**

A single exponential fit to the proton $T_{1\rho}$ relaxation data. Single exponential fit to the decay of cross-peak intensity for residues $^{B}$Q71, $^{B}$G19, $^{B}$S34, and $^{B}$V57 of unbound α-BTX is plotted as a function of the spin-lock duration. The spectra used for this analysis were recorded at 30 °C on an 800 MHz spectrometer. Errors were estimated from S/N ratios in the spectra. Fitted exponential curves are shown.

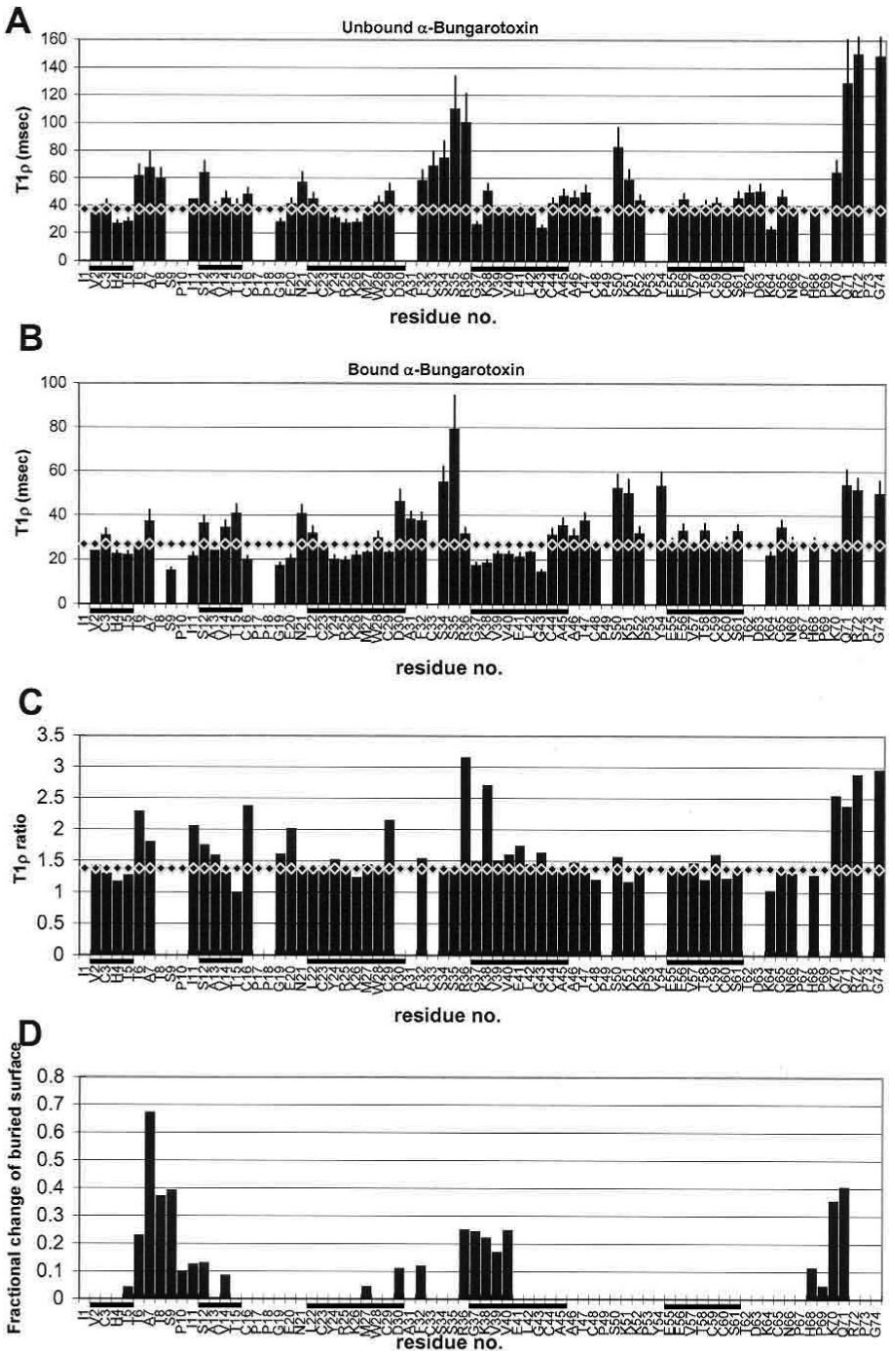


**Figure 3. Changes in $T_{1\rho}$ values of $H^{\alpha}$ protons in free and bound α-BTX**

(A) $T_{1\rho}$ values for each residue in the free toxin. Small squares denote the average $T_{1\rho}$ of β-sheets residues (37 msec). (B) $T_{1\rho}$ values for each residue in the bound toxin. Small squares denote the average $T_{1\rho}$ of β-sheets residues (28 msec). Errors in $T_{1\rho}$ values are displayed by error bars. (C) The ratio between the $T_{1\rho}$ values for each residue in the free and bound α-BTX. Small squares denote ratio between the average $T_{1\rho}$ values of the β-sheets residues in the free and bound toxin (1.32). All values were measured on the 800 MHz spectrometer at 30°C. Solid horizontal lines beneath the residue axis indicate β-sheet structure. (D) The fractional decrease in exposed surface area upon complex formation for each α-BTX residue.

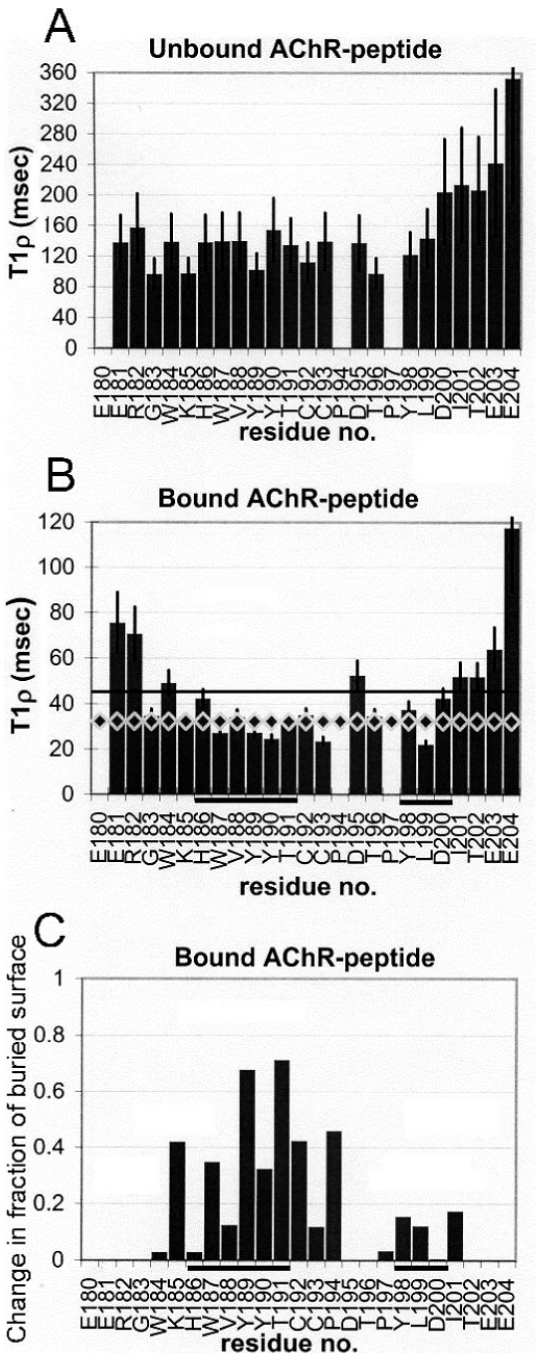


**Figure 4. Comparison between $T_{1\rho}$ values of $H^{\alpha}$ protons in free and bound AChR-peptide and changes in exposed surface upon binding**

(A) $T_{1\rho}$ values of each residue in the free AChR peptide. (B) $T_{1\rho}$ values for each residue in the AChR peptide in complex with the toxin. The spectra of the free and bound AChR peptide were measured at 30°C on 500 MHz and 800 MHz spectrometers respectively. Errors in $T_{1\rho}$ values are displayed by error bars. The average $T_{1\rho}$ value of 32.3 msec for the peptide residues in β-strands is denoted in B by small squares, and the 45 msec threshold used to differentiate between the peptide residues interacting with the toxin and those that do not is drawn by a horizontal line. (C) The fractional decrease in exposed surface for residues in the AChR-peptide. Solid lines beneath the residue axis represent β-sheet structure.

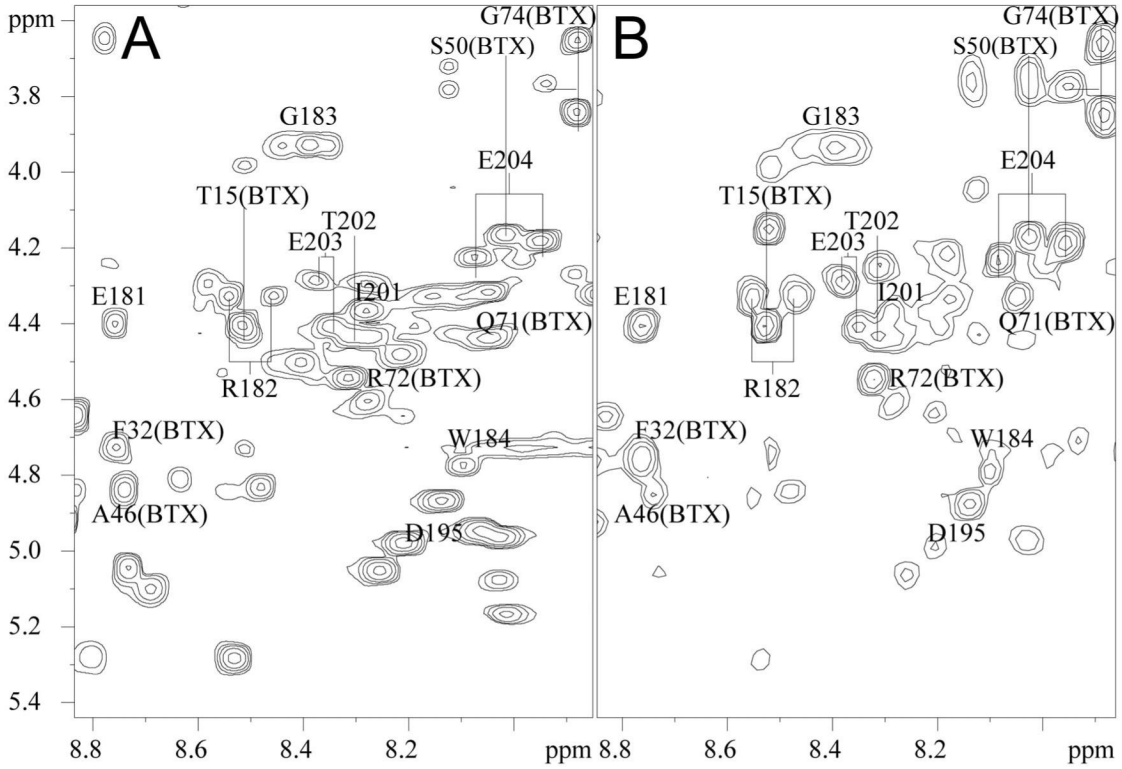


**Figure 5. $T_{1\rho}$-filtered HOHAHA spectra of the α-BTX/AChR-peptide complex measured with different durations of the WALTZ pulse train**

A) A spectrum recorded with a WALTZ pulse train and trim pulses with a total duration of 30 msec. B) A spectrum recorded with a WALTZ pulse train and trim pulses with a WALTZ pulse train and trim pulses with a total duration of 200 msec. In both experiments a spin lock with duration of 25 msec was applied after the initial 90° pulse and prior the evolution period. Notice the fewer $H^{\alpha}$ cross-peak in spectrum B in comparison with spectrum A.

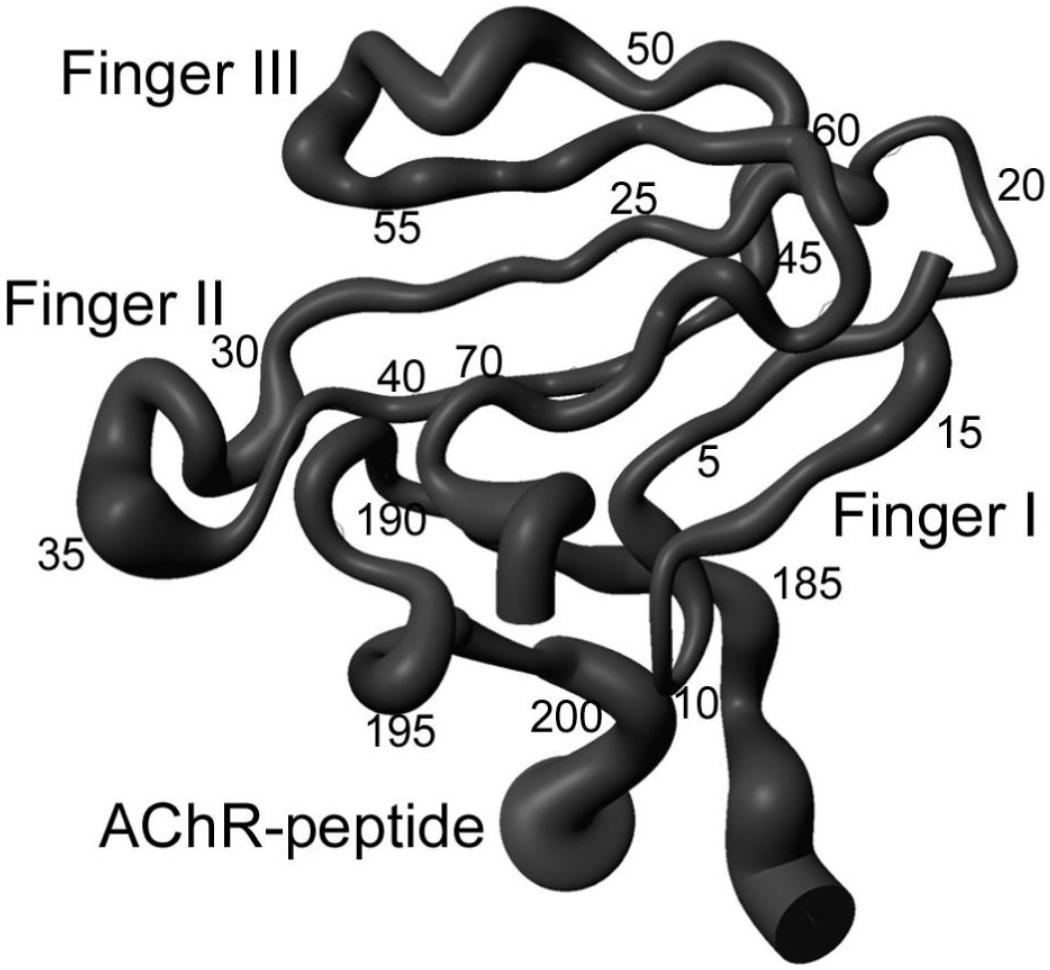


**Figure 6.**
Variation in $T_{1\rho}$ values drawn on the backbone structure of the α-BTX/AChR-peptide complex. The thickness of the $C^{\alpha}$ trace is proportional to the $T_{1\rho}$ values of the toxin and peptide residues.